Fractional Marcus-Hush-Chidsey-Yakopcic current-voltage model for redox-based resistive memory devices

Georgii Paradezhenko,[1] Dmitrii Prodan,[1] Anastasiia Pervishko,[1] Dmitry Yudin,[1] and Anis Allagui[2,3]

[1] *Skolkovo Institute of Science and Technology, Moscow 121205, Russia*
[2] *Department of Sustainable and Renewable Energy Engineering, University of Sharjah, Sharjah, P.O. Box 27272, United Arab Emirates*
[3] *Department of Mechanical and Materials Engineering, Florida International University, Miami, FL33174, United States*

(Dated: February 21, 2023)

We propose a circuit-level model combining the Marcus-Hush-Chidsey electron current equation and the Yakopcic equation for the state variable for describing resistive switching memory devices of the structure metal–ionic conductor–metal. We extend the dynamics of the state variable originally described by a first-order time derivative by introducing a fractional derivative with an arbitrary order between zero and one. We show that the extended model fits with great fidelity the current-voltage characteristic data obtained on a Si electrochemical metallization memory device with Ag-Cu alloy.

I. INTRODUCTION

Substantial research efforts have been dedicated to the development of electrically-controlled resistive switching in metal-insulator-metal (MIM) devices or memristors, going from new materials discovery[1–7] to modelling and simulation[8–10], and design and applications[3,11–13]. With both memory and logic capabilities combined at the hardware level, in addition to long retention times[11] and high switching rates[14] at relatively low energy consumption[1,15], these devices are favorably seen as the next-generation building blocks for nonvolatile memories and neuromorphic computing applications[11,12]. In a typical memristor, the resistive switching is based on the electrically-stimulated change of cell resistance usually driven by internal ion redistribution, which actually depends not only on the applied excitation but also on the past history of the excitation[6]. Physical mechanisms associated with these reversible transitions have been attributed to different effects including valence-change [16], electrochemical metallization[17], and phase change effects[18]. They can be either abrupt (binary) or gradual (analogue), and evolve at different timescales, leading to rich and complex device behaviors in this seemingly simple device structure of just three layers[19]. Furthermore, with the wide range of diversity in memristors materials and their morphologies, operating mechanisms, and manufacturing technologies there is an urgent need for the development of a general model capable of capturing accurately and effectively their complex nonlinear dynamics. This is crucial not only for the characterization and comparison between different memristor devices, but also for the investigation of larger scale memristor-based circuits and hybrid hardware architectures, and also to explore similar behaviors observed for instance in biological synapse systems[20].

While models at different size scales and thus with different degrees of physical details and computational complexity have been developed for memritors, including but not limited to *ab initio*[21], kinetic Monte Carlo, and finite element method models[22], in this work we focus on the circuit-level (compact) current-voltage behavior of memristors. From this point of view, memristors are generally described by the system of coupled equations[23]:

$$i = G(v, x)v, \tag{1}$$

$$\dot{x} = f(x, v), \tag{2}$$

where $i = i(t)$ is the current through the device, $v = v(t)$ is the applied voltage, and $x = x(t)$ corresponds to a state variable or a group of state variables that quantify the internal dynamics of the device. These are, for example, width of doping region, concentration of vacancies in the gap region, and tunneling barrier width[8]. State variables can not be observed from external electrical behavior[24]. Eq. (1) follows the i-v curve of the resistive device in question with $G(v, x)$ being the generalized conductance, whereas Eq. (2) describes the dynamics of its internal state x based on its prehistory[25]. The actual state of a memristor can only be determined by solving Eqs. (1) and (2) self-consistently. Memristive systems as featured in terms of Eqs. (1) and (2) are known to possess a pinched hysteresis loop at the origin in the i-v plane in the response to any periodic voltage source[26].

Being versatile and modular enough it is the Yakopcic model [27–29] which is most often used to simulate the nonlinear i-v characteristic of wide range of memristors in response to sinusoidal and repetitive sweeping inputs. The model takes into account electron transmission effects, voltage threshold for state variable motion, and nonlinear velocity function for oxygen vacancies or dopant drift, considered to be the most relevant internal state information[29]. It follows on the steps of Strukov *et al.* work[30], and describes the memristor as two resistors in series characterized by electron transmission equations so that[29]:

$$i(t) = h_1(v)x + h_2(v)(1 - x). \tag{3}$$

Here, h_1 is used to model the behavior in the low-resistance state of the device, and h_2 captures its behav-

ior in the high-resistance state. The two electron transmission equations are weighted and mixed by the state variable x which is set to take values between zero and one[25]. In memristive devices, it is the rate of change of the state variable x that is explicitly determined (2), and is given in the Yakopcic memristor model by the product of the two composite functions $g(v)$ and $f(x)$ such that[29]:

$$\dot{x}(t) = g(v)f(x). \tag{4}$$

An exponential dependency of the state change to the positive and negative regions of the input voltage v is modelled in terms of

$$g(v) = \begin{cases} a_p \cdot (1 - e^{u_p - v}) \cdot e^{v}, & v - u_p > 0, \\ a_n \cdot (e^{u_n + v} - 1) \cdot e^{-v}, & v + u_n < 0, \\ 0, & \text{otherwise}, \end{cases} \tag{5}$$

including programming voltage thresholds u_p and u_n. The magnitude of state change for a voltage potential is defined with a_p and a_n. The second function $f(x)$ is determined by

$$f(x) = \begin{cases} w_p(x, x_p) \cdot e^{-(x - x_p)}, & x \geq x_p, \\ 1, & x < x_p, \end{cases} \tag{6}$$

for $v > 0$, while for $v < 0$, it is defined as

$$f(x) = \begin{cases} w_n(x, x_n) \cdot e^{x + x_n - 1}, & x \leq 1 - x_n, \\ 1, & x > 1 - x_n. \end{cases} \tag{7}$$

Effectively, this function introduces the nonlinear ion motion, as it becomes harder to change the state of the devices when the state variable approaches the boundaries. In Eq. (6), $w_p(x, x_p)$ is a windowing function that ensures $f(x)$ equals zero when $x(t) = 1$, and in (7), $w_n(x, x_n)$ keeps $x(t)$ from becoming less than 0 when the current flow is reversed. These two functions can explicitly be written as $w_p(x, x_p) = 1 + (x_p - x)/(1 - x_p)$ and $w_n(x, x_n) = x/(1 - x_n)$.

Clearly, in (3), the functions h_1 and h_2 are dependent on the structure and type of memristor under study. Several types of resistive switching memory devices can be classified as nanoionic-based electrochemical systems, wherein an ion conductor in the form of electron insulator layer is placed between two electrodes[31,32]. For the case of cation-migration-based electrochemical metallization memory cells, Ag or Cu are typically used as active electrodes, Pt or W as counter electrodes, and a variety of oxides or chalcogenides thin films as solid electrolytes. When a positive voltage is applied, the active electrode material is oxidized at the electrode–electrolyte interface leading to the release of metallic ions in the adjacent electrolyte, followed by drift and diffusion of these ions across the electrolyte, and then their deposition in filamentary-like metal structures at the counter electrode surface. Short-circuit occurs when the filament has grown sufficiently far to make an electronic contact with the opposite electrode, which defines the low-resistance state of the cell. When a negative voltage is applied, the cell returns back, in principle reversibly, to the high-resistance state[31]. Anion-migration-based valence change cells, on the other hand, are formed by placing a metal oxide between for example Pt or TiN electrodes and another oxygen-affine, lower work function electrode. The low-resistance and high-resistance states are defined based on the electrochemical formation of oxygen-deficient, mixed ionic–electronic conducting filaments, and the nanoionic modification of the potential barrier between the tip of the filament and the electrode it faces[31]. For these types of redox-based resistive memory cells, it is more appropriate to consider electron transfer theory associated with the kinetics of redox reactions to better describe their i-v characteristics. Furthermore, because the formation and rupture of the metallic filaments follow random paths, the possibility of charge trapping from one operation sequence to another, charge leakage, the dynamics of an internal state variable associated with these cells cannot be defined solely based on its immediate past, in other words via integer-order derivative as in (2). Taking into account the integral past is believed to be more representative for a proper mathematical description of the complexity and dissipative nature of these cells.

Motivated by these observations, we herein propose a circuit-level model for redox-based resistive memory devices, where the current equation (1) is taken from the Marcus-Hush-Chidsey (MHC) theory[33–35] of heterogeneous electron transfer, while the state variable equation (2) is taken from the Yakopcic generalized memristive model[27]. We consider the dynamics of the state variable with respect to time to be of fractional, non-integer, order. Mathematically, this adds an extra degree of freedom to the model that can be generically correlated to the non-perfect reversibility of the device when looking at it from one cycle to another. We fit the extended model to the experimental data obtained on a Si memristor with Ag-Cu alloy as reported in[36]. A close inspection of numerical results unambiguously reveals that switching to the fractional derivative allows one to significantly improve the agreement between the theory and experimental data.

II. MEMRISTOR MODEL

The generalized i-v relationship, as specified by Eq. (1), for the proposed memristor model reads

$$i = \gamma_1 x\, h(\delta_1 v) + \gamma_2 (1 - x)\, h(\delta_2 v), \tag{8}$$

where $\delta_1, \delta_2, \gamma_1, \gamma_2 > 0$ are model parameters, and the function

$$h(v) = h_+(v) - h_-(v), \tag{9}$$

is based on the MHC model for electron transfer described by the Gauss-Fermi integral[35],

$$h_\pm(v) = \beta \int_{-\infty}^{\infty} \exp\left\{ -\frac{(z - \lambda \pm v)^2}{4\lambda} \right\} \frac{dz}{1 + e^z}. \tag{10}$$

Here, the $\pm$ signs refer to the oxidative and reductive transition rate functions, λ is the dimensionless reorganization energy scaled to $k_{\mathrm{B}}T$, while the integral over the dimensionless variable z accounts for the Fermi statistics of electron energies, distributed around the electrode potential. The prefactor β accounts for the electronic coupling strength and the electronic density of states of the electrode. In Eq. (10), λ and β are assumed to be fitting parameters, knowing that β is usually expressed as an exponential term itself that depends on the distance between the donor and acceptor of electrons. This, however, does not affect the generality of the proposed model. Finally, v in Eqs. (8)–(10) is actually the electrochemical overpotential defined as the difference between the equilibrium Nernst-potential of the metal and the actual electrode potential defined by the external power supply. We will consider the equilibrium potential to be negligible, so that the electrochemical potential is equal to the applied voltage on the device.

For the dynamics of the state variable $x(t)$, we introduce a fractional time derivative in (4) as follows,

$$D_t^{\alpha} x(t) = g(v) f(x), \qquad x(0) = x_0, \tag{11}$$

where D_t^{α} is the fractional derivative operator of order $\alpha > 0$ in the sense of Caputo,

$$D_t^{\alpha} x(t) \equiv \frac{1}{\Gamma(n-\alpha)} \int_0^t \frac{x^{(n)}(\tau) d\tau}{(t-\tau)^{\alpha+1-n}}, \tag{12}$$

where $n-1 < \alpha < n$, while $\Gamma(z) = \int_0^{\infty} t^{z-1} e^{-t} dt$ in the denominator stands for the Gamma function, and $x^{(n)}(\tau)$ is the n-th order derivative. In our follow-up study, the order of the derivative is assumed to be $0 < \alpha < 1$.

Thus, the parameters

$$\boldsymbol{p} = (\alpha, x_p, x_n, a_p, a_n, u_p, u_n, \beta, \lambda, \gamma_1, \gamma_2, \delta_1, \delta_2). \tag{13}$$

being arranged into one vector specify the proposed memristor model.

III. METHODS

A. Evaluation of the MHC integral

The Gauss-Fermi integrals like (10) can be evaluated numerically using the Gauss-Hermite quadrature (see, e.g.,[37]). In practice,

$$\int_{-\infty}^{\infty} e^{-x^2} f(x)\, dx \approx \sum_{k=1}^{n} c_k f(x_k), \tag{14}$$

where n corresponds to the amount of sample points, while x_k are the roots of the Chebyshev-Hermite polynomial $H_n(x_k) = 0$ with $k = 1, \ldots, n$. For a given $n \geq 2$ the Chebyshev-Hermite polynomial $H_n(x)$ can be identified from recurrence relations

$$H_{n+1}(x) = 2xH_n(x) - 2nH_{n-1}(x), \tag{15}$$

provided $H_0(x) = 1$ and $H_1(x) = 2x$. In (14), the coefficients c_k are given by

$$c_k = \frac{2^{n-1}}{n^2} \frac{n!}{[H_{n-1}(x_k)]^2} \sqrt{\pi}. \tag{16}$$

Thus, one can rewrite the MHC integrals (10) in the form

$$h_{\pm}(v) = 2\beta\sqrt{\lambda} \sum_{k=1}^{n} \frac{c_k}{1 + \exp\{2x_k\sqrt{\lambda} + \lambda \pm v\}}. \tag{17}$$

In our numerical simulations, the order of quadrature $n = 25$, which is deemed more than sufficient for our purpose.

B. Solution to the fractional differential equation

The nonlinear fractional differential equation (11) is solved numerically using the Adams-type predictor-corrector method[38]. For nonlinear fractional differential equations of the form

$$D_t^{\alpha} x(t) = F(t, x), \quad x^{(k)}(0) = x_0^{(k)}, \tag{18}$$

where $k = 0, 1, \ldots, m-1$ and $m = \lceil \alpha \rceil$, this method can be described as follows. The approach is based on the fact that the initial value problem is equivalent to the Volterra integral equation

$$x(t) = \sum_{k=0}^{m-1} \frac{t^k x_0^{(k)}}{k!} + \frac{1}{\Gamma(\alpha)} \int_0^t \frac{F(\tau, x(\tau))}{(t-\tau)^{1-\alpha}}\, d\tau. \tag{19}$$

We assume that the choice of $F(t, x)$ guarantees the existence of a unique solution in a certain interval $0 \leq t \leq T$. We divide this interval into N equal pieces as specified by a uniform grid at the points $t_n = hn$, $n = 0, 1, \ldots, N$ and $h = T/N$. The basic idea is that using pre-calculated approximations $x_h(t_j) \approx x(t_j)$, $j = 0, 1, \ldots, n$, we get the next time step approximation $x_h(t_{n+1})$ by means of Eq. (19).

Replacing the integral on the right-hand side of Eq. (19) by the product rectangle rule, we obtain

$$\int_0^{t_{n+1}} \frac{F(\tau, x(\tau))}{(t_{n+1}-\tau)^{1-\alpha}}\, d\tau \approx \frac{h^{\alpha}}{\alpha} \sum_{j=0}^{n} F_j \cdot b_{n-j}, \tag{20}$$

where $F_j = F(t_j, x_h(t_j))$ and $b_k = (k+1)^{\alpha} - k^{\alpha}$, provided that $0 \leq k \leq n$. The predicted value $x^P(t_{n+1})$ is determined by the fractional Adams-Bashforth method,

$$x_h^P(t_{n+1}) = \sum_{k=0}^{m-1} \frac{t_{n+1}^k x_0^{(k)}}{k!} + \frac{h^{\alpha}}{\Gamma(\alpha+1)} \sum_{j=0}^{n} F_j \cdot b_{n-j}. \tag{21}$$

To obtain a formula for the corrector, one uses the product trapezoidal quadrature formula to replace the integral in Eq. (19), where nodes t_j are taken with respect to

the weight function $(t_{n+1}-\tau)^{\alpha-1}$. Using standard techniques from quadrature theory, we can write the integral on the right-hand side of Eq. (19) as

$$\int_0^{t_{n+1}} \frac{F(\tau, x(\tau))}{(t_{n+1}-\tau)^{1-\alpha}}\, d\tau \approx \frac{h^\alpha}{\alpha(\alpha+1)} \sum_{j=0}^{n+1} F_j \cdot a_{n-j}, \quad (22)$$

where $a_{-1}=1$ and $a_n = n^{\alpha+1} - (n-\alpha)(n+1)^\alpha$, while $a_k = (k+2)^{\alpha+1} - 2(k+1)^{\alpha+1} + k^{\alpha+1}$ for $k = 1, \ldots, n-1$. We thus come to the corrector approximation, which can be thought of as the fractional variant of the one-step Adams-Moulton method,

$$x_h(t_{n+1}) = \sum_{k=0}^{m-1} \frac{t_{n+1}^k x_0^{(k)}}{k!} + \frac{h^\alpha}{\Gamma(\alpha+2)} F(t_{n+1}, x_h^P(t_{n+1})) + \frac{h^\alpha}{\Gamma(\alpha+2)} \sum_{j=0}^{n} F_j \cdot a_{n-j}. \quad (23)$$

The numerical error of this method is shown to behave as

$$\max_{j=0,1,\ldots,N} \left| x(t_j) - x_h(t_j) \right| = O(h^p), \quad (24)$$

with $p = \min\{2, 1+\alpha\}$. In practice, we first calculate and store the coefficients given by $\{b_k\}$ and $\{a_k\}$ of Eqs. (20) and (22) as arrays. After that, on each time step we calculate the predictor (21) and then use it to calculate the corrector (23). To speed up the calculations, we apply the Fast Fourier Transform algorithm to compute the convolutions on the right-hand sides of Eqs. (21) and (23).

C. Fitting method

Suppose the i-v curve is yielded by N measurements $\{\hat{t}_k, \hat{v}_k, \hat{i}_k\}_{k=1}^N$. To fit the model as specified by Eqs. (8) and (11) to this data, we search for the set of fitting parameters (13) using the least squares method. This is done by applying the Trust Region Reflective algorithm[39] to minimize the cost function,

$$\boldsymbol{p}^* = \arg\min_{\boldsymbol{p}} \sum_{k=1}^{N} \left[\hat{i}_k - i(\hat{v}_k, \hat{t}_k, x(\hat{t}_k), \boldsymbol{p}) \right]^2, \quad (25)$$

where $i(v,t,x,\boldsymbol{p})$ is the right-hand side of (8). The parameters are non-negative, and the fractional derivative order is bounded, $0 < \alpha \leq 1$. Since the current (8) depends on the state variable $x(t)$, for each $\boldsymbol{p}$ we self-consistently solve either the ordinary (4) or fractional (11) differential equation with respect to the state variable in $0 \leq t \leq T$. As long as the evolution of $x(t)$ is described in terms of the ordinary differential equation, we keep the parameter $\alpha = 1$ excluded from the fitting parameters vector (13). Eq. (4) is solved numerically using the Runge–Kutta–Fehlberg method, while Eq. (11) is addressed by a means of the Adams-type predictor-corrector method on condition that $x(0) = 0$. Once the state variable $x(t)$ is calculated, we interpolate it at time steps $\hat{t}_k$ and evaluate the current $i(v,t,x,\boldsymbol{p})$ for specific points $\{\hat{v}_k, \hat{t}_k, x(\hat{t}_k)\}_{k=1}^N$. The fitted model is then evaluated and compared to the experimental data using the Normalized Root-Mean-Square Error (NRMSE),

$$\mathrm{NRMSE} = \frac{\frac{1}{\sqrt{N}} \sqrt{\sum_{k=1}^N (i_k - \hat{i}_k)^2}}{\frac{1}{N}\sum_{k=1}^N \hat{i}_k}, \quad (26)$$

where $i_k = i(\hat{v}_k, \hat{t}_k, x(\hat{t}_k), \boldsymbol{p})$ is the evaluated model current.

Parameters	Integer order	Fractional order
α	1.000	0.697
x_p	0.000	0.619
x_n	0.000	19.17
a_p	0.711	0.071
a_n	0.108	0.006
u_p	4.796	4.718
u_n	0.000	0.000
β	0.524	1.372
λ	16.94	15.95
γ_1	4.865	1.746
γ_2	6.328	2.520
δ_1	3.947	4.121
δ_2	2.308	2.165
NRMSE	0.399	0.401

TABLE I. Fitting results for the MHC-Yakopcic model with ordinary and fractional differential equation for the state variable.

IV. RESULTS AND DISCUSSION

We fitted the memristor specified by Eqs. (8) and (11) combining the MHC-based state-controlled current-voltage relationship and the fractional Yakopcic state variable model to the i-v characteristic data of the electrochemical metallization memory device taken from[36]. The device is a Si memristor with Ag–Cu alloying conducting channels that was fabricated following the method of Yeon *et al.*[40]. For the i-v measurements that were carried out on a BioLogic VSP-300 workstation, six successive sinusoidal voltage waveforms were applied across the two terminals of the device such that

$$v(t) = u_0 \sin(2\pi f t), \quad (27)$$

with $u_0 = 6$ V and $f = 1$ Hz in the unit time interval $t \in [0,1]$. The measured i-v signals were separated into six sequences, and then averaged into a single i-v characteristic cycle on which fitting is performed.

The numerical simulations of the models with the ordinary and fractional derivatives fitted to the experimental

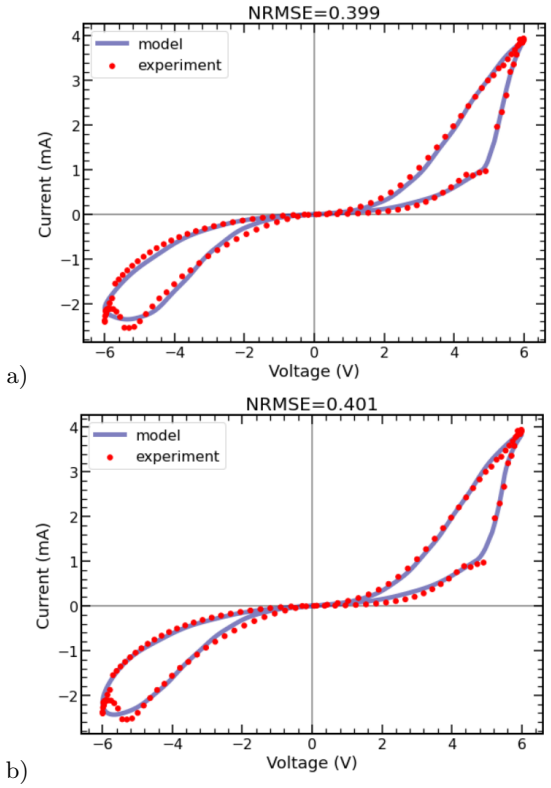

FIG. 1. Fit of the i-v characteristic calculated by the MHC-Yakopcic model to the data obtained for the memristor device developed in Skoltech, where the dynamics of a state variable is described by a) the ordinary differential equation (4) and b) the fractional differential equation (11).

i-v data are presented in Fig. 1. As mentioned above we considered the equilibrium Nernst-potential of the electrode to be zero, so that the electrochemical potential in Eqs. (8) and (11) is equal to the actual applied voltage on the device. The corresponding fitting parameters are provided in Table I. As one can see, the MHC-Yakopcic model fits very well to the experimental data with NRMSE = 0.401 for the fractional order $\alpha = 0.697$. Remarkably enough, NRMSE = 0.399 when the state variable evolves according to the ordinary differential equation, *i.e.*, with $\alpha = 1$. In comparison, the q-deformed memristor model recently reported in[36] resulted in NRMSE = 0.457. The q-deformed model was derived by taking into account gamma-distributed local spatial inhomogeneities in the device structure. This provided a noticeable improvement in the fitting of the i-v response of the same device under study here when compared to the currently used existing model (*i.e.*, the Yakopcic model with MIM and Schottky electron transmission equations)[36]. However, as mentioned above, the kinetics of electrode reactions in redox-based electrochemical metallization memory cells should be rather described by electron transfer theory.

The value of $\alpha = 0.697$ (Table I) in the fractional derivative for the state variable equation indicates that its dynamics does not evolve without prior knowledge of all past information of its state or memory of its past. This can be clearly illustrated by rewriting Eq. (21) as:

$$x_h^P(t_{n+1}) = \frac{h^\alpha}{\Gamma(\alpha+1)}\left\{F_n + \sum_{j=0}^{n-1} F_j \cdot b_{n-j}\right\} + \ldots, \quad (28)$$

which can be decoupled as the the sum of the immediate past of the state variable, and a memory trace[41], represented by the second summation term, that contains information about all previous states of the device.

The magnitude of the memory trace term increases when α decreases further away from one, and when we are close to the actual instant t at which the variable is evaluated. At the limiting case of $\alpha = 1$, corresponding to first-order integer derivative, the memory trace part vanishes, and does not have any effect on the dynamics of the state variable. Here, because $\alpha \neq 1$ we may speak of an intrinsic memory embedded in our redox-based resistive memory device. Fractional dynamics are in fact very often observed in electrochemical devices and complex systems[42–48]. Indeed, a close inspection of Table I reveals that the fractional MHC-Yakopcic memristor model is practically insensitive to the input voltage $a_p, a_n \approx 0$.

V. CONCLUSION

In this work we proposed a compact and accurate model for describing the electrical behavior of redox-based resistive memory devices in which (i) the state-controlled current-voltage equation is based on the MHC theory for electron transfer, and (ii) the dynamics of the state variable is assumed to follow fractional time derivatives of order α ($0 < \alpha < 1$). For the numerical solution to the MHC integral we used the Gauss-Hermite quadrature method and for the fractional differential equation of the state variable we used an Adams-type predictor-corrector technique. Goodness of fit to the experimental data is evaluated in terms of NRMSE, and indicates superior capabilities of the proposed model when compared to recently reported ones. The obtained results, in connection to the electrochemical nature of the device under test, point out to necessity to take into consideration fractional dynamics when describing the i-v characteristics of redox-based resistive memory devices. The fractional parameter can be viewed as an additional quantity representing the non-ideality, dissipative behavior of these devices.

[1] B. J. Choi, A. C. Torrezan, J. P. Strachan, P. G. Kotula, A. J. Lohn, M. J. Marinella, Z. Li, R. S. Williams, and J. J. Yang. High-speed and low-energy nitride memristors.

Adv. Funct. Mater., 26(29):5290–5296, 2016.

[2] C.-Y. Wang, C. Wang, F. Meng, P. Wang, S. Wang, S.-J. Liang, and F. Miao. 2d layered materials for memristive and neuromorphic applications. *Adv. Electron. Mater.*, 6(2):1901107, 2020.

[3] Y. van De Burgt, A. Melianas, S. T. Keene, G. Malliaras, and A. Salleo. Organic electronics for neuromorphic computing. *Nat. Electron.*, 1(7):386–397, 2018.

[4] Ethan C Ahn, H-S Philip Wong, and Eric Pop. Carbon nanomaterials for non-volatile memories. *Nat. Rev. Mater.*, 3(3):1–15, 2018.

[5] Vinod K Sangwan and Mark C Hersam. Neuromorphic nanoelectronic materials. *Nat. Nanotechnol.*, 15(7):517–528, 2020.

[6] S. Satapathi, K. Raj, and M. A. Afroz. Halide-perovskite-based memristor devices and their application in neuromorphic computing. *Phys. Rev. Applied*, 18(1):017001, 2022.

[7] S.-G. Xu, P. Zhang, and X. Zhang. Design of memristor materials from ordered-vacancy zincblende semiconductors. *Phys. Rev. Mater.*, 5(2):024603, 2021.

[8] N. V. Agudov, A. V. Safonov, A. V. Krichigin, A. A. Kharcheva, A. A. Dubkov, D. Valenti, D. V. Guseinov, A. I. Belov, A. N. Mikhaylov, and A. Carollo. Nonstationary distributions and relaxation times in a stochastic model of memristor. *J. Stat. Mech.: Theory Exp.*, 2020(2):024003, 2020.

[9] W. Wang, M. Laudato, E. Ambrosi, A. Bricalli, E. Covi, Y.-H. Lin, and D. Ielmini. Volatile resistive switching memory based on ag ion drift/diffusion—part ii: Compact modeling. *IEEE Trans. Electron. Devices*, 66(9):3802–3808, 2019.

[10] Kena Zhang, Jianjun Wang, Yuhui Huang, Long-Qing Chen, P Ganesh, and Ye Cao. High-throughput phase-field simulations and machine learning of resistive switching in resistive random-access memory. *Npj Comput. Mater.*, 6(1):1–10, 2020.

[11] J. J. Yang, D. B. Strukov, and D. R. Stewart. Memristive devices for computing. *Nat. Nanotechnol.*, 8(1):13–24, 2013.

[12] S. Kumar, X. Wang, J. P. Strachan, Y. Yang, and W. D Lu. Dynamical memristors for higher-complexity neuromorphic computing. *Nat. Rev. Mater.*, pages 1–17, 2022.

[13] H. Bao, Z. Hua, H. Li, M. Chen, and B. Bao. Discrete memristor hyperchaotic maps. *IEEE Trans. Circuits Syst. I: Regul. Pap.*, 68(11):4534–4544, 2021.

[14] A. C. Torrezan, J. P. Strachan, G. Medeiros-Ribeiro, and R. S. Williams. Sub-nanosecond switching of a tantalum oxide memristor. *Nanotechnology*, 22(48):485203, 2011.

[15] J. Zhou, F. Cai, Q. Wang, B. Chen, S. Gaba, and W. D. Lu. Very low-programming-current rram with self-rectifying characteristics. *IEEE Electron Device Lett.*, 37(4):404–407, 2016.

[16] H.-S. P. Wong, H.-Y. Lee, S. Yu, Y.-S. Chen, Y. Wu, P.-S. Chen, B. Lee, F. T. Chen, and M.-J. Tsai. Metal–oxide rram. *Proc. IEEE*, 100(6):1951–1970, 2012.

[17] R. Waser, R. Dittmann, G. Staikov, and K. Szot. Redox-based resistive switching memories–nanoionic mechanisms, prospects, and challenges. *Adv. Mater.*, 21(25-26):2632–2663, 2009.

[18] H.-S. P. Wong, S. Raoux, S. B. Kim, J. Liang, J. P. Reifenberg, B. Rajendran, M. Asheghi, and K. E. Goodson. Phase change memory. *Proc. IEEE*, 98(12):2201–2227, 2010.

[19] M. A. Zidan, J. P. Strachan, and W. D. Lu. The future of electronics based on memristive systems. *Nat. Electron.*, 1(1):22–29, 2018.

[20] A. Ascoli, F. Corinto, V. Senger, and R. Tetzlaff. Memristor model comparison. *IEEE Circuits Syst. Mag.*, 13(2):89–105, 2013.

[21] B. Traoré, P. Blaise, E. Vianello, L. Perniola, B. De Salvo, and Y. Nishi. Hfo_2-based rram: Electrode effects, ti/hfo_2 interface, charge injection, and oxygen (o) defects diffusion through experiment and ab initio calculations. *IEEE Trans. Electron Devices*, 63(1):360–368, 2015.

[22] S. Larentis, F. Nardi, S. Balatti, D. C. Gilmer, and D. Ielmini. Resistive switching by voltage-driven ion migration in bipolar rram—part ii: Modeling. *IEEE Trans. Electron Devices*, 59(9):2468–2475, 2012.

[23] L. Chua. Memristor-the missing circuit element. *IEEE Trans. Circuit Theory*, 18(5):507–519, 1971.

[24] Y. Shang, W. Fei, and H. Yu. Analysis and modeling of internal state variables for dynamic effects of nonvolatile memory devices. *IEEE Trans. Circuits Syst. I: Regul. Pap.*, 59(9):1906–1918, 2012.

[25] T. Chang, S.-H. Jo, K.-H. Kim, P. Sheridan, S. Gaba, and W. Lu. Synaptic behaviors and modeling of a metal oxide memristive device. *Appl. Phys. A*, 102(4):857–863, 2011.

[26] L. Chua. If it's pinched it's a memristor. In R. Tetzlaff, editor, *Memristors and Memristive Systems*, chapter 2, pages 17–90. Springer, New York, 2014.

[27] C. Yakopcic, T. M. Taha, G. Subramanyam, R. E. Pino, and S. Rogers. A memristor device model. *IEEE Electron Device Lett.*, 32(10):1436–1438, 2011.

[28] C. Yakopcic, T. M. Taha, G. Subramanyam, and R. E. Pino. Generalized memristive device spice model and its application in circuit design. *IEEE Trans. Comput.-Aided Des. Integr. Circuits Syst.*, 32(8):1201–1214, 2013.

[29] C. Yakopcic, T. M. Taha, D. J. Mountain, T. Salter, M. J. Marinella, and M. McLean. Memristor model optimization based on parameter extraction from device characterization data. *IEEE Trans. Comput.-Aided Des. Integr. Circuits Syst.*, 39(5):1084–1095, 2019.

[30] D. B. Strukov, G. S. Snider, D. R. Stewart, and R. S. Williams. The missing memristor found. *Nature*, 453(7191):80–83, 2008.

[31] I. Valov, E. Linn, S. Tappertzhofen, S. Schmelzer, J. van den Hurk, F. Lentz, and R. Waser. Nanobatteries in redox-based resistive switches require extension of memristor theory. *Nat. Commun.*, 4(1):1771, 2013.

[32] I. Valov, R. Waser, J. R. Jameson, and M. N. Kozicki. Electrochemical metallization memories—fundamentals, applications, prospects. *Nanotechnology*, 22(25):254003, 2011.

[33] C. E. D. Chidsey. Free energy and temperature dependence of electron transfer at the metal-electrolyte interface. *Science*, 251(4996):919–922, 1991.

[34] R. A. Marcus. Symmetry or asymmetry of k_{et} and i_{stm} vs. potential curves. *J. Chem. Soc., Faraday Trans.*, 92:3905–3908, 1996.

[35] Y. Zeng, R. B. Smith, P. Bai, and M. Z. Bazant. Simple formula for marcus-hush-chidsey kinetics. *J. Electroanal. Chem.*, 735:77–83, 2014.

[36] R. Konlechner, A. Allagui, V. N. Antonov, and D. Yudin. A superstatistics approach to the modelling of memristor current-voltage responses. *Physica A*, 614:128555, 2023.

[37] W. H. Press, S. A. Teukolsky, W. T. Vetterling, and B. P. Flannery. *Numerical Recipes: The Art of Scientific Computing.* Cambridge University Press, New York, 2017.

[38] K. Diethelm, N. J. Ford, and A. D. Freed. A predictor-corrector approach for the numerical solution of fractional differential equations. *Nonlinear Dyn.*, 29:3–22, 2002.

[39] M. A. Branch, T. F. Coleman, and Y. Li. A subspace, interior, and conjugate gradient method for large-scale bound-constrained minimization problems. *SIAM J. Sci. Comput.*, 21(1):1–23, 1999.

[40] H. Yeon, P. Lin, C. Choi, S. H. Tan, Y. Park, D. Lee, J. Lee, F. Xu, B. Gao, H. Wu, H. Qian, Y. Nie, S. Kim, and J. Kim. Alloying conducting channels for reliable neuromorphic computing. *Nat. Nanotechnol.*, 15(7):574–579, 2020.

[41] W. Teka, T. M. Marinov, and F. Santamaria. Neuronal spike timing adaptation described with a fractional leaky integrate-and-fire model. *PLoS Comput. Biol.*, 10(3):e1003526, 2014.

[42] V. E. Tarasov. *Fractional dynamics: applications of fractional calculus to dynamics of particles, fields and media*. Springer Science & Business Media, 2011.

[43] A. Allagui, H. Benaoum, A. S. Elwakil, and M. Alshabi. Extended rc impedance and relaxation models for dissipative electrochemical capacitors. *IEEE Trans. on Electron Devices*, 69(10):5792–5799, 2022.

[44] A. Allagui and H. Benaoum. Power-law charge relaxation of inhomogeneous porous capacitive electrodes. *J. Electrochem. Soc.*, 169(4):040509, 2022.

[45] E. Hernández-Balaguera, B. Arredondo, G. del Pozo, and B. Romero. Exploring the impact of fractional-order capacitive behavior on the hysteresis effects of perovskite solar cells: A theoretical perspective. *Commun. Nonlinear Sci. Numer. Simul.*, 90:105371, 2020.

[46] D. Zhang, A. Allagui, A. S. Elwakil, A. M. Nassef, H. Rezk, J. Cheng, and W. C. H. Choy. On the modeling of dispersive transient photocurrent response of organic solar cells. *Org. Electron.*, 70:42–47, 2019.

[47] Y. F. Luchko, M. Rivero, J. J. Trujillo, and M. P. Velasco. Fractional models, non-locality, and complex systems. *Comput. Math. with Appl.*, 59(3):1048–1056, 2010.

[48] R. Metzler and J. Klafter. The random walk's guide to anomalous diffusion: a fractional dynamics approach. *Phys. Rep.*, 339(1):1–77, 2000.